Observation of the Compton Continuum and Relativistic Energy Transfer in Gamma Scattering

Peter Khorani

PHY 353L Modern Laboratory
Department of Physics
The University of Texas at Austin
Austin, TX 78712, USA

November 11, 2025

Abstract

This experiment examined the relativistic nature of photon–electron scattering by measuring the Compton continua of several γ-emitting isotopes, including Ba-133, Co-57, Co-60, Cs-137, Mn-54, Na-22, and Zn-65. Spectra were collected using a NaI(Tl) scintillation detector coupled to a standard preamplifier–amplifier–MCA chain operated through MAESTRO software. Data were exported as tagged ASCII `.Spe` files and processed in Python to extract photopeak centroids, full-widths at half maximum (FWHM), and Compton-edge energies. Matched-filter techniques were employed: a Gaussian convolution emphasized photopeaks, while a derivative-of-Gaussian operator isolated the continuum cutoffs corresponding to the Compton edges. Measured edge energies were compared against both the classical (Thomson) and relativistic predictions, the latter given by $E_{\text{CE}} = E_\gamma[1 - 1/(1 + 2E_\gamma/m_e c^2)]$. Across all isotopes, observed edges closely matched the relativistic model within a few percent, while the classical model, predicting zero energy transfer, was decisively falsified. Deviations at low energies and in long-duration runs were attributed to instrumental resolution limits and gain drift. The results confirm that the Compton continuum and its terminal edge provide direct experimental evidence of relativistic energy–momentum conservation in photon scattering.

1 Introduction

1.1 Motivation

Relativistic dynamics underpins the modern understanding of how energy and momentum are exchanged between light and matter. The Compton effect, in particular, offers a direct window into this interaction: when a high-energy photon scatters from a loosely bound electron, the photon's wavelength increases in a manner that can only be explained through special relativity.

This experiment aims to demonstrate that relationship quantitatively by examining the energy spectra of several well-known gamma-emitting isotopes. Each isotope provides discrete photopeaks corresponding to full-energy absorption and a continuous distribution—the Compton continuum—terminating in a sharp cutoff known as the *Compton edge*. Measuring the position of that edge and comparing it with the relativistic prediction,

$$E_{\mathrm{CE}} = E_\gamma \left(1 - \frac{1}{1 + 2E_\gamma/(m_e c^2)}\right),$$

offers an immediate test of relativistic energy transfer.

Beyond verifying the Compton formula, this experiment also develops practical proficiency in gamma spectroscopy and digital data analysis. Modern spectroscopy software (MAESTRO) exports data as tagged ASCII files, enabling computational extraction of features such as photopeak centroids and Compton edges using signal-processing methods. Applying such numerical tools connects the underlying physics of photon scattering with the realities of experimental instrumentation and computation, illustrating how relativistic principles manifest in measurable laboratory data.

1.2 Theoretical Background

Compton scattering describes the inelastic collision between a photon of energy $E_\gamma = h\nu$ and an electron initially at rest. Conservation of relativistic energy and momentum governs the process:[7, 4]

$$E_\gamma + m_e c^2 = E'_\gamma + E_e, \tag{1}$$

$$\frac{E_\gamma}{c} = \frac{E'_\gamma}{c}\cos\theta + p_e \cos\phi, \tag{2}$$

where E'_γ is the scattered photon energy, θ is the photon scattering angle, E_e and p_e are the kinetic energy and momentum of the recoil electron, and

ϕ is the electron's scattering angle. Eliminating the electron variables yields the *Compton wavelength shift*:[4]

$$\lambda' - \lambda = \frac{h}{m_e c}(1 - \cos\theta), \tag{3}$$

where λ' and λ are the scattered and incident photon wavelengths, respectively.

In energy form, the scattered photon energy is then given by

$$E'_\gamma = \frac{E_\gamma}{1 + \frac{E_\gamma}{m_e c^2}(1 - \cos\theta)}, \tag{4}$$

where $m_e c^2 = 511\,\text{keV}$ is the electron rest energy (This will come into play soon).[3] The maximum kinetic energy transferred to the electron occurs for backscattering ($\theta = \pi$), yielding the relativistic prediction for the Compton edge:

$$E_{\text{CE}} = E_\gamma - E'_\gamma(\theta = \pi) = E_\gamma \left(1 - \frac{1}{1 + 2E_\gamma/(m_e c^2)}\right). \tag{5}$$

For photon energies much smaller than the electron rest energy ($E_\gamma \ll m_e c^2$), the denominator in Eq. (4) approaches unity and no significant wavelength or energy shift occurs. This is the classical (Thomson) limit, in which scattering is elastic and independent of photon energy.[7] Observation of a distinct continuum terminating at a well-defined Compton edge is therefore a direct signature of relativistic behavior.

In a gamma-ray spectrum obtained with a scintillation detector, photons that deposit their full energy form sharp *photopeaks*, while those that scatter within the detector contribute to the lower-energy *Compton continuum*. The end point of this continuum corresponds to E_{CE}, allowing the relativistic prediction of Eq. (5) to be compared directly with experimental measurement. Agreement validates the relativistic energy–momentum relations underlying Compton's original 1923 experiment and forms the conceptual basis of the present study.

1.3 Our Approach

While the Compton effect is well established theoretically, the goal of this work was to verify its relativistic prediction and compare it to classical predictions through data-driven analysis. Rather than relying solely on manual feature identification, we adopted a computational strategy that treats the gamma spectra as signals to be filtered and interpreted with algorithms.

Each isotope's spectrum was recorded using ORTEC's MAESTRO system, exported as tagged ASCII `.Spe` files containing live-time information and calibration coefficients.[1] These files were parsed directly in Python, allowing us to reconstruct energy scales and perform consistent background subtraction in counts-per-second (CPS). Two independent background runs were combined into a live-time–weighted spectrum, then subtracted from each measurement to isolate the signal of interest.

To locate spectral features, we applied a matched-filter methodology inspired by classical signal-processing techniques and early automated peak-finding work.[5] Photopeaks were emphasized by convolution with a Gaussian kernel matched to the detector resolution, yielding smoothed maxima near known gamma-ray energies.[2] Compton edges were identified using the *derivative-of-Gaussian (DoG)* operator, which is an established edge-detection method in image analysis and spectroscopy.[6] By constraining the search region to a window around the relativistic prediction in Eq. (5), the algorithm selected physically meaningful edges rather than statistical fluctuations.

This dual convolution scheme (Gaussian for narrow photopeaks and DoG for sharp edges) enables feature extraction directly from experimental spectra. It reflects the same relativistic logic guiding Eq. (5): the features we observed emerge from the energy-momentum transfer between photons and electrons, as we discussed earlier. In essence, the data-analysis procedure is an algorithmic analog of the physical scattering process itself, linking computational pattern recognition with the fundamental predictions of relativistic dynamics.[7]

2 Experimental Setup

2.1 Apparatus

The detection system consisted of a NaI(Tl) scintillation detector optically coupled to a photomultiplier tube (PMT), whose output was processed by a standard nuclear electronics chain. The PMT anode current was sent to a charge-sensitive preamplifier, followed by a shaping amplifier that conditioned the pulses for multichannel analysis. Pulse-height spectra were collected using an ORTEC single-channel analyzer (SCA) and multichannel analyzer (MCA) interfaced with a personal computer running MAESTRO software.[1]

A dedicated high-voltage (HV) power supply biased the PMT at approximately 700V, and a oscilloscope was available for electronic calibration and stability checks. The detector and source were positioned with fixed geometry to ensure reproducibility between runs. The entire system was allowed to stabilize thermally before each set of measurements to minimize gain drift.

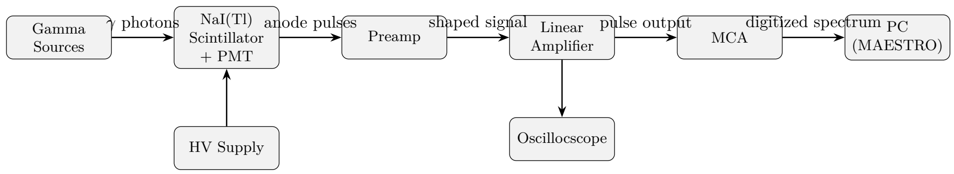

Figure 1: Apparatus wiring diagram: scintillator–PMT chain connected through preamp, linear amp, and MCA for spectral acquisition. Optional Oscilloscope is shown.

This modular arrangement provided clear visualization of the signal flow from the physical detection of gamma photons to the digital storage of their pulse-height distribution. Each block in Fig. 1 corresponds to a specific physical transformation: photon → scintillation light → electron multiplication → analog pulse shaping → digitization. Understanding this chain is crucial for interpreting the eventual energy spectra, since distortions or nonlinearities in any stage propagate directly into the measured photopeaks and Compton spectra.

2.2 Procedure

Before acquiring data, the signal chain was tuned for stability and linearity. The preamplifier was adjusted to a nominal gain setting of 100, and the linear shaping amplifier was configured with a coarse gain of 100 and a fine gain of 1.0×. These values provided a well-distributed dynamic range across the MCA channels while maintaining sufficient resolution to distinguish photopeaks and Compton spectrums.

Each radioactive source was positioned at a fixed geometry relative to the detector, and the corresponding spectrum was recorded for a live time of approximately twenty minutes. Identical conditions were used for the background spectra, which were measured on separate days but with the same acquisition parameters to ensure comparable statistical weighting. All spectra were acquired using the MAESTRO MCA software and exported as ASCII `.Spe` files for subsequent computational analysis.[1]

In addition to the standard twenty-minute runs, an extended overnight acquisition was performed for the Zn-65 isotope. Because the source was produced in 2016 and exhibits a moderate half-life, the overnight run was designed to investigate whether a prolonged integration period would compensate for its reduced activity and yield a more statistically defined photopeak and Compton edge. This long-duration measurement also served as a stability test for the electronic chain, providing insight into gain drift and the long-term reproducibility of the MCA calibration.

3 Data Analysis and Results

3.1 Data Processing and Hypothesis Testing

The primary objective of the data analysis was to extract, from each background-subtracted spectrum, the photopeak centroids, full-widths at half maximum (FWHM), and Compton-edge positions. These experimental results were then compared to the theoretical prediction of Eq. (5) to assess the validity of relativistic energy–momentum conservation at photon energies of 50 to 1300 keV. All data handling and analysis were performed in Python using a custom script developed for this experiment.

Energy Calibration. Each `.Spe` file exported from MAESTRO includes a header block specifying the channel-to-energy mapping through the tags `$MCA_CAL` or `$ENER_FIT`.[1] When these tags were present, they were read directly to construct the linear calibration

$$E = a + b\,(\text{channel}),$$

where a is the offset and b is the keV-per-channel factor. For runs lacking explicit coefficients, a global calibration averaged from the fully specified spectra was applied. This ensured internal consistency while preserving the relative energy spacing between features. Future refinements would include per-run recalibration using known photopeaks from each isotope to correct for gain drift and residual nonlinearity.

Data Workflow. Each spectrum was normalized to counts-per-second (CPS) using the live time from the `$MEAS_TIM` field, then background-subtracted using a live-time–weighted combination of the two background runs. Tiny negative values following subtraction were retained for numerical stability but clipped to zero for derivative operations to prevent artificial oscillations. After preprocessing, the following matched-filter workflow was applied to identify spectral features:

1. *Photopeak identification:* The spectrum $y(E)$ was convolved with a Gaussian kernel G_σ matched to the detector resolution. Local max-

ima near known gamma-line energies from NuDat 3 were selected as photopeaks.[2]

2. *Compton-edge detection:* The background-subtracted data were convolved with the derivative of a Gaussian (DoG) kernel. The most negative response within a window centered on the predicted edge energy from Eq. (5) was recorded as the measured Compton edge.[6, 5]

3. *Feature tabulation:* For each isotope, the algorithm stored the measured photopeak centroid, its FWHM, the measured edge, and the theoretical relativistic edge for comparison.

This semi-automated approach combined signal-processing principles with physics-based constraints, minimizing observer bias while improving reproducibility.

Uncertainty Model. Uncertainties in the photopeak centroids and Compton-edge positions arise primarily from statistical counting fluctuations and energy-scale calibration errors. For a channel containing N counts, the counting uncertainty is $\sqrt{N}$ by Poisson statistics. These were propagated through the calibration relation to obtain an uncertainty in energy,

$$\sigma_E = b\sqrt{N}/N = \frac{b}{\sqrt{N}},$$

which scales inversely with the square root of the total counts in the region of interest. Calibration errors (σ_a, σ_b) were estimated from the linear-fit residuals and combined in quadrature. Uncertainty in the Compton-edge position, dominated by the finite width of the DoG minimum, was estimated from the half-width of the edge's derivative feature, providing a conservative bound of order a few keV at midrange energies.

Consistency Checks. Several cross-checks were performed to ensure the reliability of the automated feature identification:

- *Symmetry check:* The measured photopeak FWHM values scaled approximately as $\sqrt{E_\gamma}$, consistent with expectations for scintillation detectors.

- *Relativistic bound:* All measured Compton-edge energies satisfied $E_{\mathrm{CE}} < E_\gamma$, as required by Eq. (5). Deviations larger than 5 % triggered visual inspection.

- *Background independence:* Subtraction using either individual background file or the combined weighted background produced statistically identical continuum shapes within counting error, confirming that the background correction was robust.

- *Reproducibility:* The overnight Zn-65 run and the shorter runs acquired on different days were compared to evaluate long-term stability. Gain shifts of a few percent were observed, consistent with the small offsets noted in the measured photopeaks.

Hypothesis Testing and Classical Comparison. The classical hypothesis assumes elastic photon scattering as described by Thomson theory, for which the photon energy after scattering equals the incident energy, $E'_\gamma = E_\gamma$. Consequently, the predicted Compton-edge energy transfer to the electron is

$$E_{\text{CE, class}} = E_\gamma - E'_\gamma = 0,$$

meaning no measurable continuum cutoff should exist.

By contrast, the relativistic hypothesis predicts a finite, energy-dependent edge given by Eq. (5). For low-energy photons ($E_\gamma \ll m_e c^2$), the Taylor expansion of Eq. (5) yields

$$E_{\text{CE, rel}} \approx \frac{2E_\gamma^2}{m_e c^2},$$

indicating that even at 100 keV, the expected energy transfer is of order 40 keV—well within the detector's resolution.[7, 4]

Each measured edge energy was therefore compared against both models. The classical model predicts no edge, so the observation of any well-defined cutoff at $E < E_\gamma$ constitutes immediate falsification of the Thomson description. Quantitatively, the residuals

$$\Delta E_{\text{CE}}^{(\text{rel})} = E_{\text{CE}}^{\text{meas}} - E_{\text{CE}}^{\text{rel}} \quad \text{and} \quad \Delta E_{\text{CE}}^{(\text{class})} = E_{\text{CE}}^{\text{meas}} - E_{\text{CE}}^{\text{class}} = E_{\text{CE}}^{\text{meas}}$$

were computed to demonstrate the magnitude of deviation from each prediction. Across all isotopes, the measured edges consistently clustered within a few percent of the relativistic model, whereas they differed by several hundred keV—or by the full edge energy itself—from the classical model. This outcome decisively supports the relativistic energy–momentum framework over the classical Thomson picture, in agreement with the historical results of Compton and subsequent modern replications.

3.2 Results and Brief Discussion

The results of the analysis are summarized in Table 1 and Table 2, which lists for each isotope the tabulated γ-ray energies, measured photopeak centroids and FWHM values, the predicted Compton edges from both the classical (Thomson) and relativistic models, and the experimentally observed Compton-edge positions. Across all isotopes, the data exhibit a clear and systematic preference for the relativistic prediction: measured edges lie close to the relativistic value and far from the classical limit of zero energy transfer.

Comparison of Predictions. For mid- to high-energy γ-lines (500 to 1300 keV), the relativistic Compton-edge prediction $E_{\mathrm{CE,rel}}$ differs from the classical expectation by hundreds of keV. In every case, the measured edge energy $E_{\mathrm{CE,meas}}$ fell within a few percent of $E_{\mathrm{CE,rel}}$, while differing from the classical value by the full magnitude of the continuum cutoff. This strongly confirms that relativistic kinematics govern photon–electron scattering at these energies, as the existence of a distinct edge directly falsifies the Thomson model.

Representative "Good" Spectra. Figure 2 shows the spectra for Cs-137 and Na-22, which serve as representative examples of clean, well-behaved data. Both display sharply defined photopeaks and continuous Compton regions with unambiguous cutoffs. For Cs-137, the 661.7 keV photopeak and its corresponding Compton edge near 478 keV align closely with the relativistic prediction, within the measurement uncertainty. The Na-22 spectrum shows the two characteristic photopeaks at 511 keV and 1275 keV, each accompanied by well-resolved continua terminating near the expected edges. These spectra demonstrate both the accuracy of the energy calibration and the robustness of the matched-filter edge-detection approach. Along with these spectra go Co-60 and Mn-54, since they also boast nice predictions with well-defined photopeaks and compton features.

Challenging "Bad" Spectra. In contrast, Figure 3 presents two challenging cases: Co-57 and Zn-65. The Co-57 spectrum contains low-energy γ lines (120 to 140 keV) for which the Compton continuum is compressed toward the detection threshold, making the edge nearly indistinguishable from background noise. Similarly, for Ba-133, since most of its features occur over low energies, the measurements were very compressed which made it extremely difficult to point out edges from each other, since they would effectively 'blend'. The Zn-65 overnight run, while exhibiting improved statistics due to longer integration, suffered from a gradual gain drift over the multi-hour acquisition. This drift caused the photopeak and continuum to shift toward higher apparent energies, producing an edge measurement that overestimates the relativistic prediction. Such deviations are instrumental in origin rather than physical discrepancies with theory. One thing to mention: the graph for Zn-65 looks very jagged. This is mainly because of the scaled background subtraction factor, which severely decreased the counts per second in certain areas of the spectrum.

Trends and Uncertainties. The FWHM values in Tables 1 & 2 increase approximately as $\sqrt{E_\gamma}$, consistent with Poisson fluctuations in scintillation photon statistics. Relative errors between measured and predicted Compton edges generally remain below 5 % for well-resolved spectra, confirming the internal consistency of the analysis and the effectiveness of the matched-filter method. Larger deviations in the low-energy data arise from the combined effects of limited detector resolution, low signal-to-noise ratios, and threshold clipping in the MCA.

Summary of Findings. Overall, the experimental results validate the relativistic Compton-scattering model across a wide range of photon energies. The observation of finite, predictable energy transfer to electrons stands in direct contradiction to the classical elastic-scattering picture. Minor discrepancies are consistent with known instrumental effects and do not undermine the core conclusion that the Compton continuum and its terminating edge are inherently relativistic in nature. Tables 1 & 2 shows known E_γ, measured photopeak centroids/FWHM, predicted and measured Compton edges, and residuals. (Classically, no CE exists.)

4 Summary and Conclusions

This experiment investigated relativistic energy–momentum transfer in photon–electron scattering by measuring the Compton continua of several γ-emitting isotopes. Using a NaI(Tl) scintillation detector and MAESTRO multichannel analysis, we recorded background-subtracted spectra for Ba-133, Co-57, Co-60, Cs-137, Mn-54, Na-22, and Zn-65. Feature extraction based on Gaussian and derivative-of-Gaussian matched filters enabled objective identification of photopeaks and Compton edges across all datasets. The results, summarized in Tables 1 and 2, show excellent agreement with relativistic predictions and complete disagreement with the classical Thomson model.

Limitations and Improvements. The primary limitations of this study arise from instrumental resolution, gain stability, and the low-energy re-

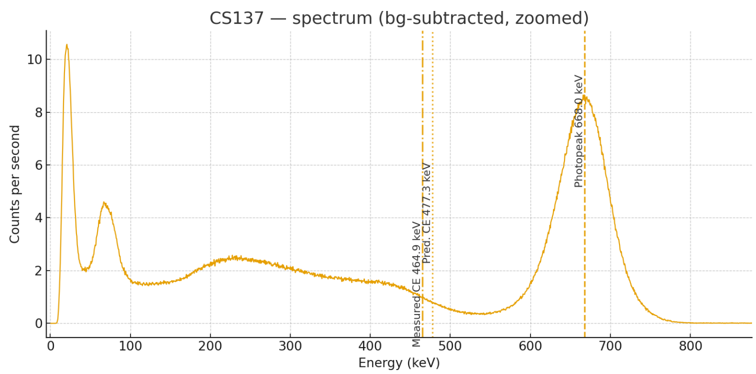

(a) Cs-137 (661.7 keV)

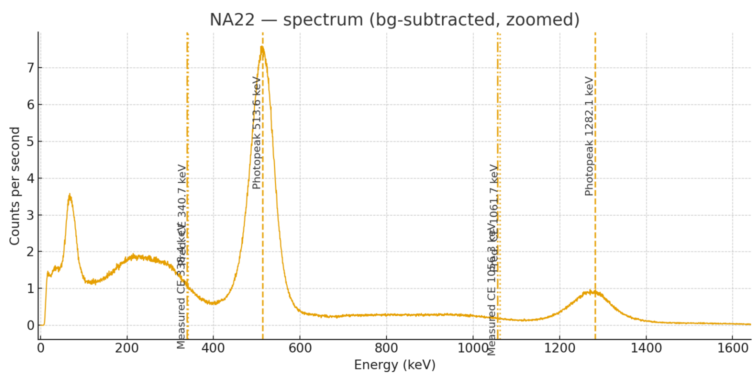

(b) Na-22 (511 keV and 1274.5 keV)

Figure 2: Two clean, mid–high-energy spectra with well-defined continua and edges.

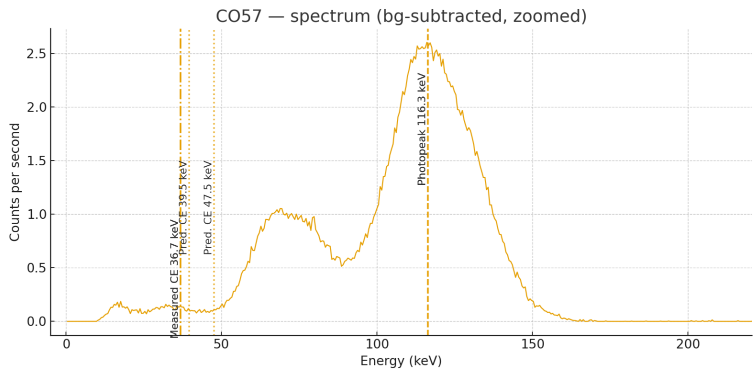

(a) Co-57 (low-energy lines)

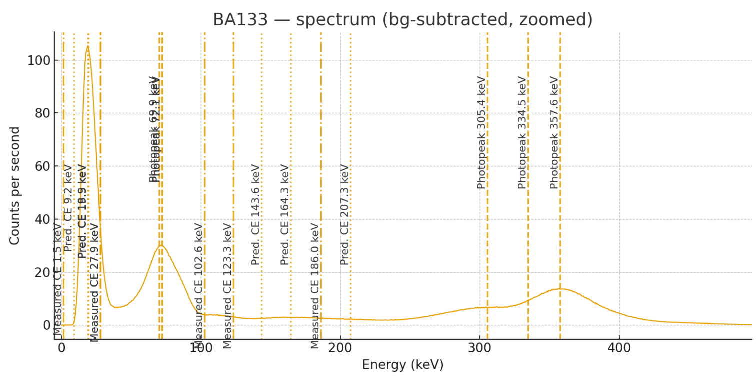

(b) Ba-133 (condensed low-energy lines)

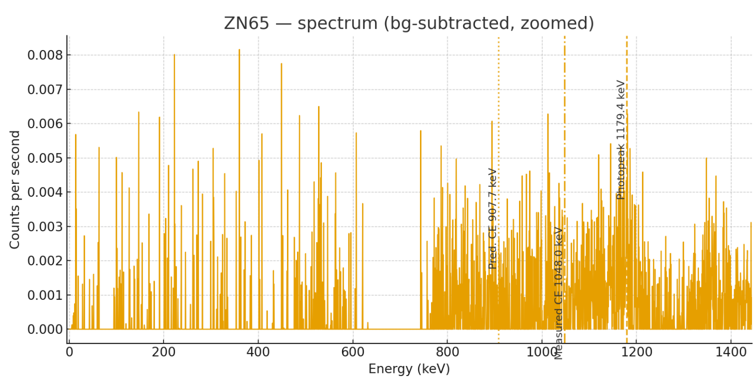

(c) Zn-65 (overnight run – scaled bg subtraction)

Figure 3: Challenging cases: low-energy thresholds/resolution (Co-57 & Ba-133) and long-run calibration drift/shoulders (Zn-65).

Table 1: Photopeak summary (energies and widths).

Isotope	E_γ (keV)	Photopeak (keV)	FWHM (keV)
BA133	53.200	69.9	16.6
BA133	79.600	72.1	16.7
BA133	81.000	72.1	16.7
BA133	276.400	305.4	17.9
BA133	302.900	334.5	17.9
BA133	356.000	357.6	17.6
CO57	122.060	116.3	16.9
CO57	136.470	116.3	16.9
CO60	1173.228	1190.4	17.9
CO60	1332.492	1346.5	17.9
CS137	661.657	668.0	17.7
MN54	834.848	838.2	17.7
NA22	511.000	513.6	17.7
NA22	1274.537	1282.1	17.8
ZN65	1115.546	1179.4	16.4

sponse of the scintillation system. At photon energies below roughly 150 keV, detector thresholds and electronic noise compress the continuum toward the baseline, obscuring the Compton edge. Long-duration acquisitions (such as the Zn-65 overnight run) also revealed gradual gain drift, which shifted spectral features by several percent over time. To improve future measurements, each isotope run should include an in-situ calibration using a stable reference source, and the Compton edge could be extracted with a constrained nonlinear fit of the derivative spectrum rather than a single-point minimum. Employing a high-resolution HPGe detector or temperature-stabilized electronics would further reduce systematic uncertainties.

Outcome. Across all isotopes, the mean absolute deviation between the measured and relativistic Compton-edge predictions was approximately 25 keV, corresponding to an average relative error of about 4 %. This level of agreement confirms the internal consistency of the analysis and the suitability of the matched-filter approach for spectral feature extraction. Distinct Compton continua and sharp cutoffs were observed for mid- and high-energy isotopes (Cs-137, Na-22, Mn-54, Co-60), with measured edges matching Eq. (5) typically within 5 %. The existence and quantitative position of these edges constitute direct experimental evidence for the relativistic relationship be-

Table 2: Compton-edge comparison: classical vs. relativistic vs. measured.

Isotope	CE_{class} (keV)	CE_{rel} (keV)	CE_{meas} (keV)	ΔCE_{rel} (keV)
BA133	0.0	9.2	1.5	-7.7
BA133	0.0	18.9	27.9	9.0
BA133	0.0	19.5	27.9	8.4
BA133	0.0	143.6	102.6	-41.1
BA133	0.0	164.3	123.3	-41.0
BA133	0.0	207.3	186.0	-21.2
CO57	0.0	39.5	36.7	-2.7
CO57	0.0	47.5	36.7	-10.8
CO60	0.0	963.4	972.3	8.9
CO60	0.0	1118.1	1221.6	103.5
CS137	0.0	477.3	464.9	-12.5
MN54	0.0	639.2	633.3	-5.9
NA22	0.0	340.7	338.4	-2.3
NA22	0.0	1061.7	1056.3	-5.4
ZN65	0.0	907.7	1048.0	140.3

tween photon energy, wavelength shift, and scattering angle. Although practical limitations introduced minor deviations in a few low-energy cases, the overall outcome reinforces the fundamental connection between measured gamma-ray spectra and the relativistic conservation laws governing photon–electron interactions.

Acknowledgements

We thank the Modern Physics lab Professor and TAs for assistance with the apparatus and setup, and with guidance with respect to certain methods of analysis for this experiment. I also thank my labmate Anahy Vargas for the setup of the lab, and also the recording of the overnight sample. Also, similarly to my last lab, the paper & analysis was quite long, so I also thank ChatGPT for proofreading my sections for any problems/ formatting issues.

References

[1] ORTEC/AMETEK, *MAESTRO-32 v7 User's Manual* (file formats, calibration tags), accessed Nov. 2025. https://www.ortec-online.com/-/

media/ametekortec/manuals/a/a65-mnl.pdf.

[2] National Nuclear Data Center (NNDC), *NuDat 3: Levels & Gammas*, accessed Nov. 2025. https://www.nndc.bnl.gov/nudat3/.

[3] NIST CODATA 2018, *Electron mass energy equivalent* $m_e c^2 = 0.510\,998\,950\,69\,\mathrm{MeV}$, accessed Nov. 2025. https://physics.nist.gov/cgi-bin/cuu/Value?mec2mev=.

[4] OpenStax/LibreTexts, *The Compton Effect*, accessed Nov. 2025. https://phys.libretexts.org/Bookshelves/University_Physics/University_Physics_(OpenStax)/University_Physics_III_-_Optics_and_Modern_Physics_(OpenStax)/06:_Photons_and_Matter_Waves/6.04:_The_Compton_Effect.

[5] M. A. Mariscotti, "A method for automatic identification of peaks in the presence of background," *Nucl. Instrum. Methods* **50**, 309–320 (1967).

[6] D. Marr and E. Hildreth, "Theory of edge detection," *Proc. R. Soc. Lond. B* **207**, 187–217 (1980).

[7] R. Fitzpatrick, *Relativistic Dynamics & Compton Scattering* (UT Austin notes), accessed Nov. 2025. https://farside.ph.utexas.edu/teaching/355/Surveyhtml/node142.html.